Activation of antiferromagnetic domain switching in exchange-coupled Fe/CoO/MgO(001) systems

Q. Li, G. Chen, T. P. Ma, J. Zhu, A. T. N'Diaye, L. Sun, T. Gu, Y. Huo, J. H. Liang, R. W. Li, C. Won, H. F. Ding, Z. Q. Qiu, and Y. Z. Wu

Phys. Rev. B **91**, 134428 — Published 29 April 2015

DOI: 10.1103/PhysRevB.91.134428

Activation of antiferromagnetic domain switching in exchange coupled Fe/CoO/MgO(001) systems

Q. Li[1], G. Chen[2], T. P. Ma[1], J. Zhu[1], A. T. N'Diaye[3], L. Sun[1], T. Gu[1], Y. Huo[1], J. H. Liang[1], R. W. Li[4], C. Won[5], H. F. Ding[6], Z. Q. Qiu[7#] and Y. Z. Wu[1*]

[1]Department of Physics, State Key Laboratory of Surface Physics and Collaborative Innovation Center of Advanced Microstructures, Fudan University, Shanghai 200433, People's Republic of China

[2]NCEM, Molecular Foundry, Lawrence Berkeley National Laboratory, Berkeley, CA 94720, United States

[3]Advanced Light Source, Lawrence Berkeley National Laboratory, Berkeley, CA 94720, United States

[4]Chinese Acad Sci, Ningbo Inst Mat Technol & Engn, Key Lab Magnet Mat & Devices, Ningbo 315201, Zhejiang, People's Republic of China

[5]Department of Physics, Kyung Hee University, Seoul 130-701, Republic of Korea

[6]National Laboratory of Solid State Microstructures, Department of Physics and Collaborative Innovation Center of Advanced Microstructures, Nanjing University, 22 Hankou Road, Nanjing 210093, People's Republic of China

[7]Department of Physics, University of California at Berkeley, Berkeley, California 94720, USA

ABSTRACT

In contrast to the extensive study of domain reversal in ferromagnetic materials, domain switching process in antiferromagnets is much less studied due to the difficulty of probing antiferromagnetic spins. Using a combination of hysteresis loop, Kerr microscope, and x-ray magnetic linear dichroism measurements, we investigated AFM domain switching process in single crystalline Fe/CoO bilayers on MgO(001). We demonstrate that the CoO AFM switching is a Kolmogorov-Avrami process in which the thermal activation energy creates AFM domain nucleation centers which further expand by domain wall propagation. From the temperature- and thickness-dependent measurements, we are able to retrieve quantitatively the important parameter of the CoO AFM activation energy, which is shown to increase linearly with CoO thickness.

Ⅰ. Introduction

Dynamics of magnetization reversal is a critical issue to both high performance spintronics technology and fundamental understanding of magnetism [1,2,3,4,5]. Although ferromagnetic(FM) materials have been the main focus of magnetism research, antiferromagnetic(AFM) materials (one of the two basic magnetic materials) have also been widely applied to magnetic recording technology [6,7]. Recently, it has been found that the AFM spin configuration can significantly influence the transport properties of the devices based on AFM materials [8,9,10,11,12,13], thus there is an increasing effort to develop modern spintronic devices using AFM materials. Since spintronics technology usually involves different spin configurations and their switching, AFM spin switching process has become one of the critical issues in developing future high performance of AFM based spintronics technology. Unfortunately, there has been very limited studies and knowledge on the AFM spin switching process.

Since AFM materials alone respond little to external magnetic field, the AFM spin switching and other functionalities usually manifest through interfacial magnetic coupling in FM/AFM heterostructures. In polycrystalline FM/AFM systems, the spin rotation and evolution of the AFM grains have been observed indirectly in the exchange bias during magnetic field cycling and are phenomenologically referred to the training effect [14,15,16,17,18,19,20,21,22]. However, the random spin orientations of AFM polycrystalline grains prohibit it to retrieve a clear physical picture on the AFM spin switching process in FM/AFM systems. To understand the AFM switching process, single crystalline AFM films have been employed recently. Shpyrko et al. [23] pioneered the measurement on an antiferromagnetic Cr single crystal using x-ray photon correlation spectroscopy. From the noise spectra, they were able to retrieve the information on the Cr spin fluctuations. However, such fluctuations are related to the spontaneous thermal and electronic excitations rather than to the FM/AFM interaction which is more relevant to spintronics technology. Using element-specified X-ray Magnetic Linear Dichroism (XMLD) to directly measure the CoO spins in single crystalline CoO/Fe bilayers, Wu et al. identified the

rotatable and frozen CoO AFM spins in thin- and thick-film limits [24], but could not explore the CoO spin switching process due to the limitation of XMLD measurement. This remains a mystery of the AFM spin switching process and its thermal activation in FM/AFM systems. In this paper, we report our study on the switching process of AFM CoO spins in single-crystalline Fe/CoO/MgO(001) system. We find that the CoO spin switching proceeds with an initial nucleation center formation followed by domain wall propagation. We show that this process is governed by the Kolmogorov-Avrami process which depends on the thermal activation energy. By temperature- and thickness-dependent studies, we retrieved the important parameter of the activation energy which depends linearly on the AFM CoO film thickness.

Ⅱ. Experiments

MgO(001) substrates were prepared in an ultrahigh vacuum system by annealing at 600 ^{o}C followed by a 10 nm MgO seed layer deposition at 500 ^{o}C. CoO film was then grown by evaporating Co under an oxygen pressure of 1.0×10^{-6} Torr at room temperature. Subsequently, an Fe film was grown on top of the CoO layer. Sharp reflection high energy electron diffraction (RHEED) patterns reveal excellent epitaxy growth of the Fe and CoO films with the lattice relation of Fe[100]//CoO[110]//MgO[110] [25,26]. The Fe/CoO/MgO(001) sample was capped with a 3nm MgO protection layer. Magnetic properties of the films were measured by longitudinal magneto-optic Kerr effect (MOKE) with a laser diode (wavelength 670 nm, beam diameter ~ 0.2 mm). The sample temperature can be varied between 82 K and 330 K in a small optical Dewar cooled by liquid Nitrogen. Magnetic domain images were taken by a commercial Kerr microscopy. XMLD experiments were performed at beamline 4.0.2 and 6.3.1 of the Advanced Light Source with the total electron yield mode.

Ⅲ. Results and discussion

Figure 1(a) shows the representative MOKE hysteresis loops of Fe (23 nm)/CoO (5 nm)/MgO(001) after field cooling to 82K with the cooling field H_{FC} parallel and

perpendicular to the MOKE optical plane, respectively. The H_{FC} was along the CoO<110> direction which is the easy axis (EA) of the in-plane four-fold anisotropy of the CoO film grown on MgO(001) [26]. Then the spin-flop Fe/CoO interfacial coupling [27,28] aligns the CoO AFM spins S_{CoO} perpendicularly to the H_{FC} and subsequently induces an in-plane uniaxial magnetic anisotropy in the Fe film with the EA parallel to H_{FC} [25,26]. This is verified by the square EA loop for $H//H_{FC}$ and the zero remanent double-split hard-axis (HA) loop for $H \perp H_{FC}$ [25]. The uniaxial magnetic anisotropy disappears above 200K where the CoO spins become rotatable to follow the Fe magnetization directional change [24]. Due to the compensated spins on CoO(001) surface, the exchange bias is negligible in Fe/CoO/MgO(001) as compared to the much stronger uniaxial anisotropy. The most surprising result is that in an intermediate temperature range, the hysteresis loop for $H \perp H_{FC}$ changes gradually from the HA loop to the EA loop with the increase of magnetic field cycling [Fig. 1(b)]. This result shows clearly that the cycling of the magnetic field gradually switched the Fe uniaxial anisotropy with its easy axis from $EA//H_{FC}$ to $EA \perp H_{FC}$.

To understand the MOKE results, we performed magnetic domain imaging measurements using a Kerr microscope on a sample of Fe (25 nm)/CoO (4 nm)/MgO(001) [Fig. 2]. The sample was first cooled down with $H_{FC}//y$ to align the CoO spins to $S_{CoO}//x$, where x and y correspond to the CoO[110] and [$1\bar{1}0$] axis, respectively. Then the remanent domain images (Fig. 2) were taken after applying a positive field $+H$ (top row) and a negative field $-H$ (bottom row) at different numbers of field cycles along the Fe hard axis ($H//x$). Right after the field cooling, only single domain with $M_{Fe}//y$ was observed [Figs. 2(a),(f)]. After the field cycling, domains with $M_{Fe}//x$ gradually appeared and expanded with the increase in cycling number. Eventually, the original single domain of $M_{Fe}//y$ was

completely switched to the final single domain of $M_{Fe}//x$ [Figs. 2(e), (j)], confirming the hysteresis loop result that the easy-axis of the Fe uniaxial anisotropy switched by 90^o through the field cycling along the original Fe hard axis. Moreover, the Kerr imaging result shows that such switching is a result of microscopic domain switching, i.e., the continuous magnetic remanence change in Fig. 1(b) is a result of increased magnetic domains with $M_{Fe}//x$. We also note that within each field cycle the domains with $M_{Fe}//+x$ in the $+H \to 0Oe$ process (light color domains in the top row of Fig. 2) are the same as to the domains with $M_{Fe}//\text{-}x$ in the $-H \to 0Oe$ process (dark color domains in the bottom row of Fig. 2), indicating that the Fe domains are pinned locally by the underlaying CoO spins, which have only uniaxial but no unidirectional order [29]. Since the Fe and CoO spins are strongly locked together, we conclude that the observed Fe domain switching is a result of the underlaying CoO AFM switching during the field cycles. The scenario is that as the Fe magnetization rotates from its original $M_{Fe}//y$ easy axis to the $M_{Fe}//x$ easy axis by the external field, the Fe/CoO interface coupling favors the CoO spins to switch from its original $S_{CoO}//x$ axis to the $S_{CoO}//y$ axis. Once the CoO AFM spins are thermally excited to switch their spins to the new lower energy state of $S_{CoO}//y$ to form a local CoO AFM domain, the Fe/CoO interfacial coupling should switch the Fe easy axis from its original y-axis to the x-axis. Therefore the 90^o-switching of Fe domains, appeared as the domain nucleation and wall propagation in Fig. 2, should originate from the CoO AFM domain switching, and the remanent Kerr signal in Fig. 1(b) should correspond to the fractional area of the switched CoO AFM domains. This fractional change [Fig. 1(c)] increases slowly with the cycling number at the beginning, faster in the middle, and then slowly again to approach the final saturation value of 1. This trend is very different from the training effect in exchange bias, which usually exhibits a dramatic decrease in the first few cycles [14-17].

We then performed XMLD measurements at the Co^{2+} L_3 edge to directly probe the CoO AFM spins in a sample of MgO (2 nm)/Fe (3 nm)/CoO (3.5 nm)/ MgO(001). After cooling the sample to 180 K with a 1 kOe field along the CoO [110] axis, the x-ray adsorption spectrum (XAS) was taken at the normal incidence of the x-rays with the polarization *E* parallel and perpendicular to H_{FC}, respectively [inset of Fig. 3(a)]. As the external magnetic field sweeps repeatedly between -700 Oe to +700 Oe in the $H \perp H_{FC}$ direction, the XMLD effect was measured after each cycle of the field sweeping. Based on the L_3 line shape analysis [30], the opposite line shapes of the CoO L_3 edge XAS before and after the field cycling [Figs. 3(a) and 3(b)] show that the CoO in-plane AFM spins are initially aligned perpendicular to H_{FC} and switched to the H_{FC} direction after the field cycling. The L_3 edge XMLD effects (R_{L_3}) [30,31] for $E//H$ and $E \perp H$ (defined as the ratio of the XAS intensity at 776.8 eV and 779.4 eV) cross each other as a function of the field cycling number and eventually saturate at the reversed values, indicating a 90^o-switching of CoO AFM spins [Fig. 3(c)]. The R_{L_3} difference between $E//H$ and $E \perp H$ cases [e.g., $\Delta R_{L_3} = R_{L_3}(E//H) - R_{L_3}(E \perp H)$] should be a quantitative measure of the areal difference between the AFM domains with the CoO spins along [110] and [$1\bar{1}0$] directions. Then the evolution of ΔR_{L_3} from negative to positive [Fig. 3(d)] values as a function of the field cycling number clearly confirms the CoO domain switching, supporting that the evolution of the Kerr remanence in Fig. 1(c) indeed comes from CoO AFM domain switching.

To understand the mechanism of AFM switching process, we investigated the temperature dependent properties of CoO AFM spin switching. Figure. 4(a) shows the Kerr remanence as a function of field cycle number *N* at different temperatures. The AFM switching time is roughly doubled when decreasing the temperature only by 1 K, showing a strong temperature dependence of the AFM spin switching. So far there exists only limited knowledge of AFM domain. There was one attempt in explaining

the exchange bias relaxation in which the growth of AFM domains were assumed within a reversed magnetic field [14]. Noticing that any domain formation and growth should involve the process of nucleation and growth which is governed by the Kolmogorov-Avrami process [14,32,33], we applied this idea to the case of the Fe/CoO/MgO(001) system where thermal activations should break the original CoO single domain into multi-domains in the form of $\sim \exp\left[-(t/\tau)^{\sigma}\right]$, where t is time, σ is a power index, and τ is the relaxation time constant [14]. Since the ratio between the remanence signal (M_r) and the saturation signal (M_S) along the original Fe hard axis measures the area of the switched CoO domains, we establish an exponential relation between the CoO domain switching process and the remanence ratio in Fig. 1(c) based on the Kolmogorov-Avrami process,

$$M_r(N)/M_s = 1-\exp(N/\tau_D)^{\sigma}. \quad (1)$$

Here N is the number of field cycles, and τ_D is the relaxation time constant with the identical time unit cost in each loop scan (~10 s for each loop cycle). To test the validity, we use Eq. (1) to fit the Kerr remanence in Fig. 1(c) and Fig. 4(a). The result shows an excellent agreement of Eq. (1) with the experimental data. Furthermore, ΔR_{L_3} in the XMLD measurement denotes the area difference between the un-switched and the switched CoO AFM domains, thus should follow the expression of

$$\Delta R_{L_3} = \Delta R_0(2\exp(-N/\tau_D)^{\sigma}-1). \quad (2)$$

Here ΔR_0 is the maximum L_3 ratio difference at the initial single domain state after field cooling. We find that Eq. (2) indeed well describes the experimental curve in Fig. 3(d). Therefore both MOKE and XMLD measurements prove the validation of the Kolmogorov-Avrami process in describing AFM CoO switching process.

Figs. 4(b) and 4(c) show the τ_D and σ values as a function of temperature from the data fitting of Fig. 4(a). While the value of $\sigma \sim 3$ shows little temperature dependence, τ_D value decreases exponentially with the Arrhenius law of [3]:

$$\tau_D = \tau_0 \exp(E_V / k_B T) . \quad (3)$$

Here τ_0 is a characteristic attempt time with the time unit cost in each loop scan, E_V is the energy barrier of the CoO AFM domain with the activation volume V, T is the temperature used in the measurements, and k_B is the Boltzmann constant. By fitting the results of Fig. 4(b), we obtain the energy barrier of $E_V = 0.91eV$ for 4.5 nm CoO film.

The CoO energy barrier E_V was further studied by obtaining the relaxation time τ_D and the power index σ at different temperatures and CoO thicknesses [Figs. 5(a) and 5(b)]. The index σ is ~3 for CoO thickness less than 5 nm and then decreases for thicker CoO films. For the reversal dynamics of FM domains, a value of $\sigma \sim 3$ corresponds to a domain wall motion dominated process [1,5]. Thus we attribute our $\sigma \sim 3$ value at thinner CoO films to the domain wall motion mechanism of the CoO domain switching process, which is consistent with the domain images in Fig. 2. For thicker CoO film, σ decreases to 1, indicating that the domain switching is dominated by the domain nucleation process [1,5]. The energy barrier E_V [Fig. 5(c)], obtained by fitting τ_D in Fig. 5(a) using Eq. (3), shows a linear dependence on CoO thickness. Since the CoO spins rotate uniformly across the CoO thickness [24], the energy barrier E_V should be proportional to the CoO crystalline anisotropy energy within the activation volume $V = d_{CoO} A_{act}$, where A_{act} stands for the activation area of the CoO domain and d_{CoO} is the CoO film thickness. Therefore, the linear thickness-dependence of the energy barrier suggests that the activation AFM domain area is independent of CoO thickness.

In addition to the CoO magnetic anisotropy, our CoO 90^o domain switching occurs with the Fe magnetization aligned in its original hard axis so that the Fe/CoO interfacial coupling benefits the CoO switching. Therefore the overall energy barrier for the 90^o-switching of a CoO domain should be:

$$E_V = K_c d_{CoO} A_{act} - K_{ex} A_{act} . \quad (4)$$

Here K_c denotes the cubic anisotropy energy density of CoO film, K_{ex} is the in-plane uniaxial anisotropy energy density induced by the Fe/CoO exchange coupling. Eq. (4) yields a vanishing of the energy barrier E_V at the critical thickness of $d_c = K_{ex} / K_c$. Indeed we found that there exists a critical CoO thickness of d_c~2.7nm below which the double-split HA loop becomes square EA loops for both $H \perp H_{FC}$ and $H // H_{FC}$ directions [Fig. 5(d)]. Taking d_c~2.7nm, M_s=1714 emu/cm^3 for Fe magnetization, and $K_{ex} = H_s M_s d_{Fe} \sim 1.34 erg / cm^2$ [25] where the shift field H_s~340 Oe is the offset of the minor loop of the HA double-split loop [Fig. 1(a)], K_c is estimated to be $5.0\times10^6 erg / cm^3$ which is much smaller than the volume cubic anisotropy of $2.7\times10^8 erg / cm^3$ in bulk AFM CoO crystal [6]. The smaller anisotropy could be attributed to the strain effect or the finite size effect in thin AFM film. Moreover, Eq. (4) also shows that the linear slope of the activation energy versus the CoO thickness corresponds to $K_c A_{act}$. Then from the linear slope of $\sim 0.54 eV / nm$ in Fig. 5(c) and K_c, we further obtained the activation area A_{act} of the AFM domain nucleation to be ~173 nm^2, which corresponds to a circle of radius r_c ~7.4 nm. This radius determines the minimum size of the AFM domain creation, in which the CoO AFM spins switch coherently.

Ⅳ. Summary

In summary, we investigated the AFM domain 90^o-switching process in epitaxial grown Fe/CoO/MgO(001). Magnetic domain images show that AFM domain switching occurs through domain nucleation plus domain wall propagation. The AFM domain relaxation can be well described by the Kolmogorov-Avrami process with the temperature-dependent relaxation time being well described by the Arrhenius law. The energy barrier of the CoO domain switching was retrieved experimentally, which was

found to increase linearly with CoO thickness above a critical thickness. This linear dependence is a result of competition between the CoO cubic anisotropy and the Fe/CoO interface exchange coupling.

ACKNOWLEDGMENTS

This work was supported by the National Key Basic Research Program (No. 2015CB921401, No. 2011CB921801) of China, the National Science Foundation of China (No. 11274074, No. 11434003, No. 11474066), National Science Foundation DMR-1210167, and National Research Foundation of Korea Grant funded by the Korean Government (2012R1A1A2007524). XMLD measurements were performed at the Advanced Light Source, Lawrence Berkeley National Laboratory, supported by the Office of Science, Office of Basic Energy Sciences, Scientific User Facilities Division, of the US Department of Energy under Contract number DE-AC02—05CH11231.

FIGURES

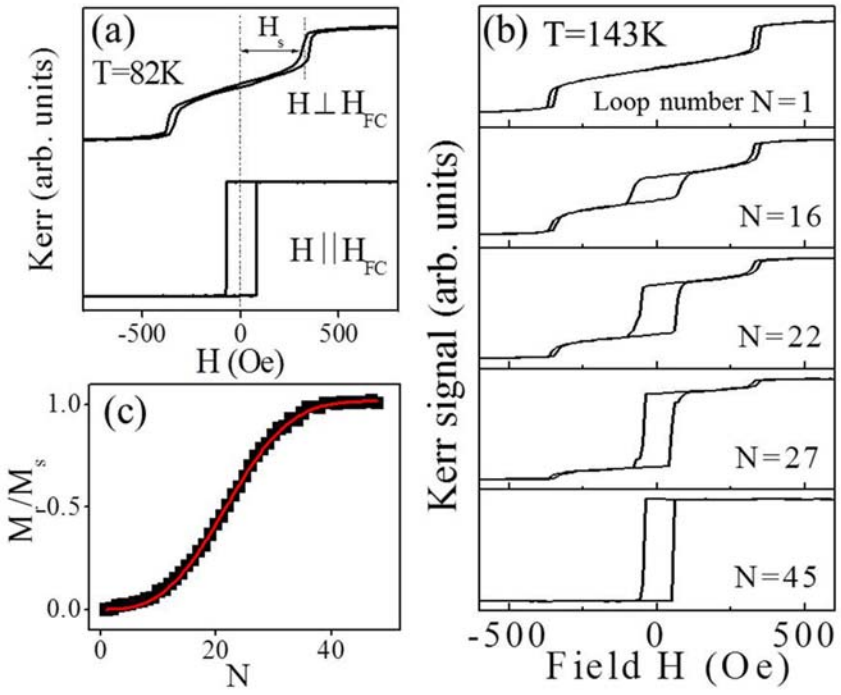

Fig. 1. (a) Hysteresis loops for $H \perp H_{FC}$ and $H // H_{FC}$ from Fe (23 nm)/CoO (5 nm)/MgO(001) at 82K. (b) Representative hysteresis loops for $H \perp H_{FC}$ at 143K during magnetic field cycling (N denotes the cycling number). (c) Remanent Kerr signal in (b) increases with the cycling number. The red line in (c) is the fitting result using Eq. (1).

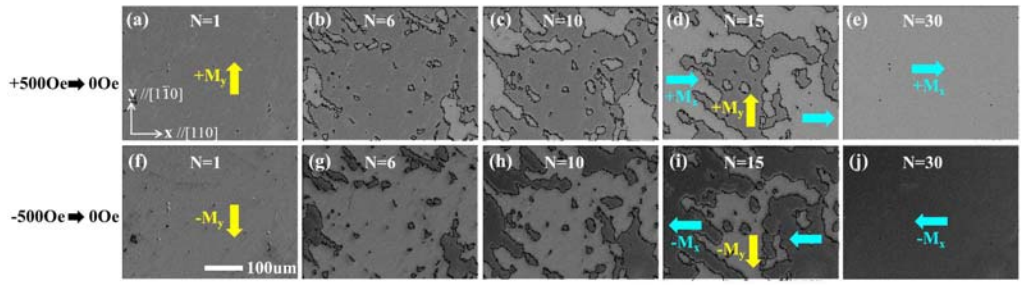

Fig. 2. Time-dependent domain evolution of Fe (25 nm)/CoO (4 nm)/MgO(001) at remanent state after different numbers of field cyclings at 144 K with (a-e) H decreased from a positive field (+500 Oe) and (f-j) H decreased from a negative field (−500 Oe). The cycling number *N* is listed in each frame. Domain boundaries are plotted using black lines as a visual guide.

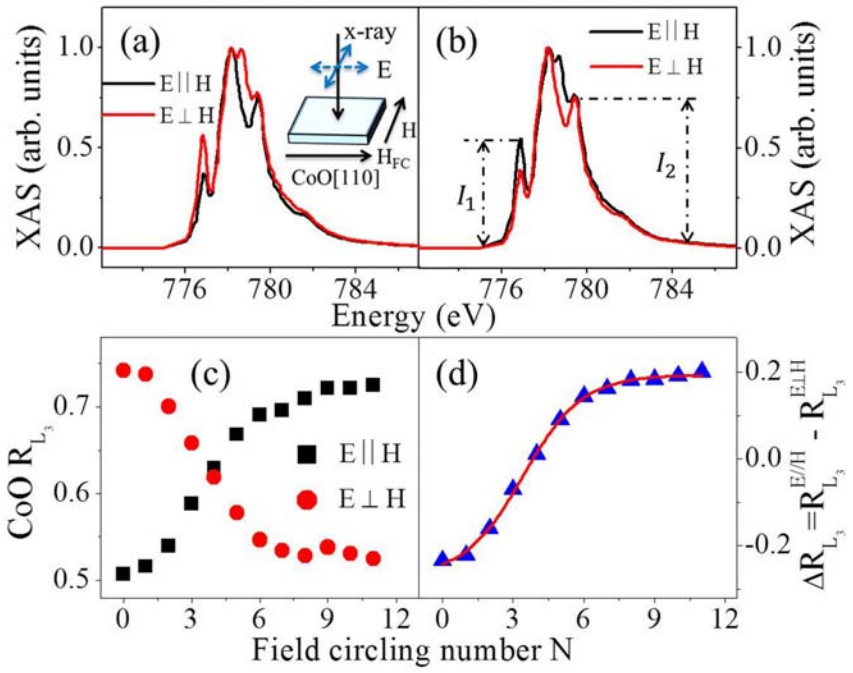

Fig. 3. CoO x-ray absorption spectrum at L_3 edge with the x-ray beam polarization $E//H$ and $E\perp H$ (a) before and (b) after field cycling at 180 K from Fe (3 nm)/CoO (3.5 nm)/MgO(001). The insert in (a) indicates the XMLD measurement geometry. (c) CoO R_{L_3} ratio versus field cycling number for both beam polarization $E//H$ and $E\perp H$ at 180 K. (d) The R_{L_3} difference ΔR_{L_3} between $E//H$ and $E\perp H$ as a function of cycling number. The red line in (d) is the fitted result using Eq. (2).

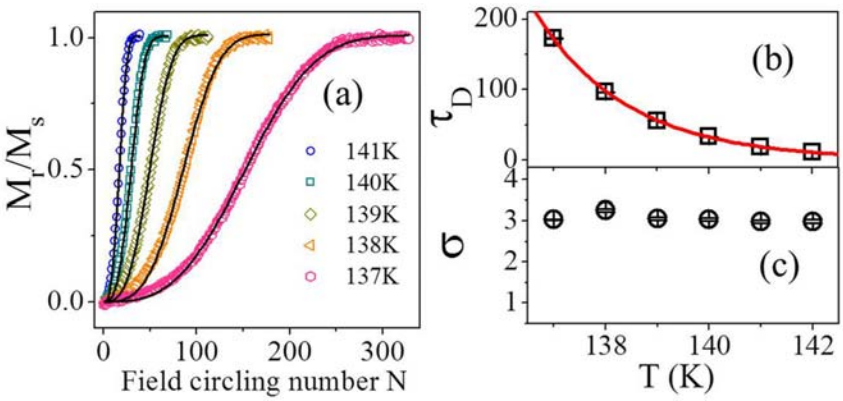

Fig. 4. (a) Remanent Kerr signal versus field cycling number N at different temperatures from the sample of Fe (23 nm)/CoO (4.5 nm)/MgO(001). The black lines are the fitted results using Eq. (1). (b) and (c) Temperature dependent relaxation time constant τ_D and the fitted exponent σ, respectively. Red line in (b) is the fitted result using Eq. (3) based on the Arrhenius law.

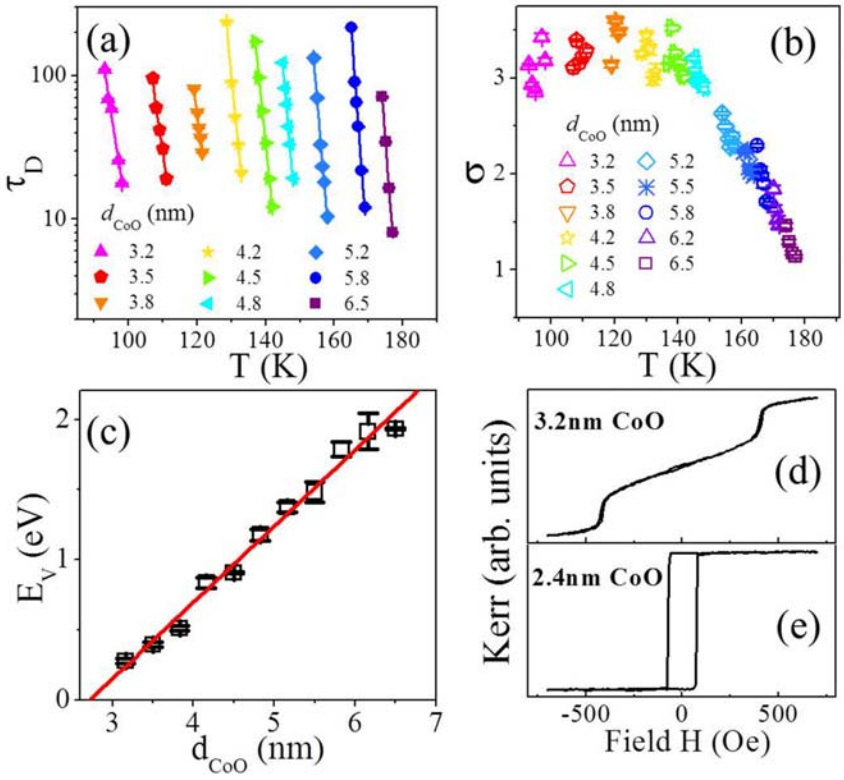

Fig. 5. (a) and (b) Temperature dependent relaxation time constant τ_D and the fitted exponent σ for Fe (23 nm)/CoO step/MgO(001) with various CoO thicknesses. Lines are fitted results using Eq. (3). (c) The energy barrier from the fitting as a function of the CoO thickness. (d) and (e) Typical loops measured at 82 K with the applied field of $H \perp H_{FC}$ for the samples with CoO thickness of 3.2 nm and 2.4 nm, respectively.

Electronic address: qiu@berkeley.edu
* Electronic address: wuyizheng@fudan.edu.cn

1 J. Pommier, P. Meyer, G. Penissard, and J. Ferre, P. Bruno, and D. Renard, Phys. Rev. Lett. **65**, 2054 (1990).

2 Sug-Bong Choe and Sung-Chul Shin, Phys. Rev. Lett. **86**, 532 (2001).

3 W. Wernsdorfer, E. Bonet Orozco, K. Hasselbach, A. Benoit, B. Barbara, N. Demoncy, A. Loiseau, H. Pascard, and D. Mailly, Phys. Rev. Lett. **78**, 1791 (1997).

4 M. Yamanouchi, J. Ieda, F. Matsukura, S. E. Barnes, S. Maekawa, H. Ohno, Science **317**, 1726 (2007).

5 H. W. Xi, K.-Z. Gao, J. O. Yang, Y. M. Shi and Y. Z. Yang, J. Phys. Condens. Matter **20**, 295220 (2008).

6 J. Nogués and I. K. Schuller, J. Magn. Magn. Mater. **192**, 203 (1999).

7 C. Chappert, A. Fert and F. Nguyen Van Dau, Nat. Mater. **6**, 813 (2007).

8 A. H. MacDonald and M. Tsoi, Phil. Trans. R. Soc. A **369**, 3098 (2011).

9 B. G. Park, J. Wunderlich, X. Martí, V. Holý, Y. Kurosaki, M. Yamada, H. Yamamoto, A. Nishide, J. Hayakawa, H. Takahashi, A. B. Shick and T. Jungwirth, Nat. Mater. **10**, 347 (2011).

10 Y. Y. Wang, C. Song, B. Cui, G. Y. Wang, F. Zeng, and F. Pan, Phys. Rev. Lett. **109**, 137201 (2012).

11 X. Marti, I. Fina, C. Frontera, J. Liu, P. Wadley, Q. He, R. J. Paull, J. D. Clarkson, J. Kudrnovský, I. Turek, J. Kuneš, D. Yi, J-H. Chu, C. T. Nelson, L. You, E. Arenholz, S. Salahuddin, J. Fontcuberta, T. Jungwirth and R. Ramesh, Nat. Mater. **13**, 367 (2014)

12 Z. Wei, A. Sharma, A. S. Nunez, P. M. Haney, R. A. Duine, J. Bass, A. H. MacDonald, and M. Tsoi, Phys. Rev. Lett. **98**, 116603 (2007).

13 S. Urazhdin and N. Anthony, Phys. Rev. Lett. **99**, 046602 (2007).

14 H. W. Xi, Scott Franzen, S. N. Mao, and Robert M. White, Phys. Rev. B **75**, 014434 (2007).

15 J. Dho, C. W. Leung, and M. G. Blamire, J. Appl. Phys. **99**, 033910 (2006).

16 P. A. A. van der Heijden, T. F. M. M. Maas, W. J. M. de Jonge, J. C. S. Kools, F. Roozeboom, Appl. Phys. Lett. **72**, 492 (1998).

17 S. Polisetty, S. Sahoo, and C. Binek, Phys. Rev. B **76**, 184423 (2007).

18 A. Hoffmann, Phys. Rev. Lett. **93**, 097203 (2004).

19 S. Brems, K. Temst, and C. V. Haesendonck, Phys. Rev. Lett. **99**, 067201 (2007).

20 B. F. Miao, J. H. Ai, L. Sun, B. You, An Hu, and H. F. Ding, Phys. Rev. B **82**, 134442 (2010).

21 T. R. Gao, D. Z. Yang, S. M. Zhou, R. Chantrell, P. Asselin, J. Du and X. S. Wu, Phys. Rev. Lett. **99**, 057201 (2007).

22 X. P. Qiu, D. Z. Yang, S. M. Zhou, R. Chantrell, K. O'Grady, U. Nowak, J. Du, X. J. Bai, and L. Sun, Phys. Rev. Lett. **101**, 147207 (2008).

23 O. G. Shpyrko, E. D. Isaacs, J. M. Logan, Y. J. Feng, G. Aeppli, R. Jaramillo, H. C. Kim, T. F. Rosenbaum, P. Zschack, M. Sprung, S. Narayanan and A. R. Sandy, Nature, **447**, 68 (2007).

24 J. Wu, J. S. Park, W. Kim, E. Arenholz, M. Liberati, A. Scholl, Y. Z. Wu, Chanyong Hwang, and Z. Q. Qiu, Phys. Rev. Lett. **104**, 217204 (2010).

25 J. Zhu, Q. Li, J. X. Li, Z. Ding, C. Y. Won, and Y. Z. Wu, J. App. Phys. **114**, 173912 (2013).

26 W. N. Cao, J. Li, G. Chen, J. Zhu, C. R. Hu, and Y. Z. Wu, Appl. Phys. Lett. **98**, 262506 (2011).

27 N. C. Koon, Phys. Rev. Lett. **78**, 4865 (1997).

28 T. C. Schulthess and W. H. Butler, Phys. Rev. Lett. **81**, 4516 (1998).

29 F. Nolting, A. Scholl, J. Stöhr, J. W. Seo, J. Fompeyrine, H. Siegwart, J.-P. Locquet, S. Anders, J. Lüning, E. E. Fullerton, M. F. Toney, M. R. Scheinfeink and H. A. Padmore, Nature **405**, 767 (2000).

30 G. van der Laan, E. Arenholz, R. V. Chopdekar, and Y. Suzuki, Phys. Rev. B **77**, 064407 (2008).

31 J. Zhu, Q. Li, J. X. Li, Z. Ding, C. Y. Hua, M. J. Huang, H.-J. Lin, Z. Hu, C. Won, and Y. Z. Wu, J. Appl. Phys. **115**, 193903 (2014).

32 A. N. Kolmogorov, Izv. Akad. Nauk SSSR, Ser. Mat. **3**, 355 (1937).

33 M. Avrami, J. Chem. Phys. **8**, 212 (1940).